Applied Surface Science 258 (2012) 7813–7819

Contents lists available at SciVerse ScienceDirect

Applied Surface Science

journal homepage: www.elsevier.com/locate/apsusc

A white-emitting ZnO–Au nanocomposite and its SERS applications

Lanlan Sun, Dongxu Zhao*, Meng Ding, Haifeng Zhao, Zhenzhong Zhang, Binghui Li, Dezhen Shen

State Key Laboratory of Luminescence and Applications, Changchun Institute of Optics, Fine Mechanics and Physics, Chinese Academy of Sciences, 3888 East Nan-Hu Road, Open Economic Zone, Changchun 130033, People's Republic of China

ARTICLE INFO

Article history:
Received 23 February 2012
Received in revised form 5 April 2012
Accepted 5 April 2012
Available online 11 April 2012

Keywords:
ZnO–Au
Hybrid
White-emitting
SERS

ABSTRACT

We reported a simple method to synthesize ZnO–Au nanocomposites (hybrid A) by combining hydrothermal and electric beam evaporation deposition method. It was found that Au deposition time takes an important role in the generation of Au nanoparticles. Changing Au deposition time makes the thickness of Au formed on ZnO nanorods increase from 10 nm to 70 nm. On the other hand, white-emitting ZnO–Au nanocomposites (hybrid B) were obtained after treating hybrid A with HCl solution. Thanks to the covering of Au film and acid etching, it induces many defects on the surface of ZnO NRs, and largely enhances the visible emission of surviving ZnO and finally generates white emission on Au mesocrystals (hybrid B). Both of the ZnO–Au hybrids (A and B) can be applied as substrates in surface-enhanced Raman scattering (SERS) measurement. A typical probe molecule, 4-ATP was used to test the SERS activity of the ZnO–Au composites and the results indicated good Raman activity on the substrates.

1. Introduction

The hybrid nanomaterials that comprise two or more different components have attracted much attention due to their unique shape- and composition-dependent properties and multiple functionalities, which are not usually achievable in single-component nanomaterials [1–3]. The multiple functionalities and even novel properties make the hybrid nanomaterials achieve applications in diverse areas, such as multimodal catalysis, biological detection, and optoelectronic applications [4–6]. The hybrid nanomaterials are usually classed as two types, the core-shell and heterodimer structures [7,8]. For core-shell hybrids, Dabbousi et al. have reported a general method for producing (CdSe)ZnS core-shell quantum dots (QDs) [9]. More recently, Au–ZnO hybrid nanoparticles have been explored based on a seed-mediated growth process [10]. For heterodimer hybrids, $Zn_{0.9}Co_{0.1}O$–Ag heterodimer nanocrystals have been synthesized and found abnormally large room-temperature ferromagnetism. Among these hybrid nanomaterials, semiconductor–noble metal hybrid nanocomposites have become an active frontier because of their remarkable optical, electrical, and catalytic properties [11–14].

ZnO, which has a wide band gap (3.37 eV) and a large exciton binding energy (60 meV), has potential photonic applications in the visible and the near-UV wavelength regions [15]. And Au nanoparticles (NPs) have great potential to complement ZnO nanorods (NRs) in constructing functional nanocomposites, because Au NPs are resistant to surface oxidation, catalytically active, and optically sensitive. Therefore, Au–ZnO hybrid nanostructures have attracted intense attention due to their potential applications in biological detection, photocatalysis, and solar cells [16–18]. Recently, Wu and co-workers have reported the photoluminescence (PL) of ZnO nanowires (NWs)-Au NPs hybrid nanostructures fabricated by attaching Au NPs onto ZnO NWs [19]. They synthesized Au NPs with different sizes by chemical reduction method, and attached Au NPs onto the surface of ZnO NWs by incubating ZnO NWs with Au NPs solutions. In their work, it is found that 40 nm Au NP is most effective in quenching the green emission and enhancing the UV emission. Sun et al. fabricated ZnO–Au NRs by a hydrothermal method and found that ZnO NRs exhibited weaker UV and visible emission when modified with Au NPs [20]. However, most of these hybrids are obtained in solution phase, thus the impurities (including chemical precursors, and capping reagent) are always introduced into the hybrids inevitably. In addition, the immersion of as-synthesized ZnO NRs into solutions may influence the photoluminescence of ZnO.

In this work, we successfully prepared ZnO–Au hybrid nanostructures by combining hydrothermal method and electric beam evaporation deposition technology. The as-synthesized ZnO–Au hybrid nanostructures (hybrid A) possess uniform Au NPs on ZnO surface. The thickness of Au NPs on ZnO surface is controllable by tuning the Au deposition time. The ZnO–Au hybrids were treated with diluted hydrochloric acid (HCl) solution and the white-emitting ZnO–Au nanocomposites (hybrid B) were obtained. The PL of the hybrid B depends on the thickness of Au NPs on ZnO surface. By comparing hybrids prepared with different Au deposition time, we found that the hybrid (B4) fabricated with Au deposition

* Corresponding author. Tel.: +86 431 86176322; fax: +86 431 4627031.
E-mail address: dxzhao2000@yahoo.com.cn (D. Zhao).

0169-4332/$ – see front matter © 2012 Elsevier B.V. All rights reserved.
http://dx.doi.org/10.1016/j.apsusc.2012.04.039

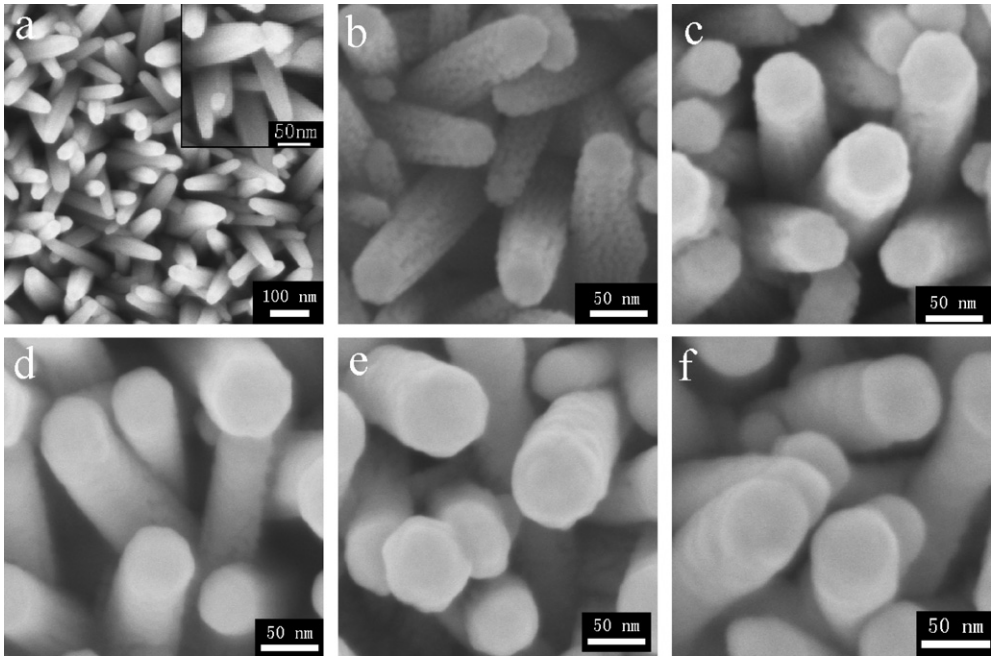

Fig. 1. SEM images of (a) ZnO NRs and ZnO–Au hybrid A with different Au deposition times, (b) 2 min, (c) 4 min, (d) 6 min, (e) 8 min, (f) 10 min.

time of 4 min exhibits the highest white emission. In addition, it is found that these ZnO–Au hybrids can be used as good SERS-active substrates with 4-aminothiophenol (4-ATP) as a test probe.

2. Experimental

2.1. Materials

Zinc acetate dehydrate ($ZnAc_2{\cdot}2H_2O$) and 4-aminothiophenol (4-ATP) were purchased from Aldrich. Hexamethylene tetramine (HMT) was purchased from Exciton Chemical Co. Inv. (Dayton, OH). Zinc nitride ($Zn(NO_3)_2$, A.R) and hydrochloric acid (HCl) were purchased from Beijing chemical reagent factory (Beijing, China). All of these chemicals and materials were used as received. Ultrapure water was used throughout the work.

2.2. Preparation of ZnO NRs

ZnO NRs arrays were prepared according to the method of Lee et al. with some modifications [21]. Briefly, cleaned indium-tin-oxide (ITO) slide was wet with a droplet of 0.02 M $ZnAc_2{\cdot}2H_2O$ in ethanol, rinsed with ethanol after 25 s, and blown dry with N_2. This wetting procedure was repeated three more times, and the sample was heated to 350 °C in air for 20 min in order to obtain ZnO seeds layers. The ITO slide with ZnO seeds was then vertically immersed into a growth solution (0.025 M $Zn(NO_3)_2$, 0.025 M HMT) and heated to 92.5 °C for 1 h. It should be indicated that the surface area of ITO slides is about 1 cm^2. For control experiment, different substrates have been used for growing ZnO nanorods, for example, glass, n-type Si (1 0 0) and sapphire substrates.

2.3. Preparation of ZnO–Au hybrid nanostructures

ZnO–Au hybrid nanostructures (hybrid A) were prepared by an electric beam evaporation deposition method with different deposition time (2 min, 4 min, 6 min, 8 min, 10 min). The detailed experimental condition is: electric current is kept at 8 mA, and the vacuum degree is kept at 10^{-2} mbar. The hybrid B was fabricated by incubating the hybrid A with diluted HCl solution (1 mM) for 3 min. Then the hybrid 2 was washed with water and dried under N_2 before characterization.

2.4. SERS measurement

Hybrids A and B were used as SERS substrates for SERS measurement. 4-ATP solution was diluted to 1×10^{-7} M with ethanol. Then, 20 μL of such solution was dropped onto the SERS substrate, and the solvent was allowed to evaporate under ambient conditions. In this experiment, more than five SERS-active substrates of each ZnO–Au hybrids were prepared, and ten different points on each substrate were selected to detect the 4-ATP probe, to verify the stability and reproducibility of these SERS active substrates.

2.5. Instruments

The morphology and structure properties of samples were investigated by field-emission scanning electron microscopy (FESEM, Hitachi S-4800), energy-dispersive X-ray spectroscopy (EDS, GENE SIS 2000 XMS 60S, EDAX, Inc.) XRD data were collected on a D/max-RA X-ray spectrometer (Rigaku). Photoluminescence (PL) measurements were performed using a He–Cd laser line of 325 nm as the excitation source. SERS spectra were measured with a Renishaw 2000 model confocal microscopy Raman spectrometer with a CCD detector and a holographic notch filter (Renishaw Ltd., Gloucestershire, U.K.). The microscope attachment was based on a Leica DMLM system, and a 50× objective was used to focus the laser beam onto a spot with approximately 1 μm in diameter. Radiation of 514.5 nm from an air-cooled argon ion laser was used for the SERS excitation. All of the spectra reported were the results of a single 20 s accumulation.

3. Results and discussion

3.1. Preparation and characterizations of ZnO and ZnO–Au hybrids (hybrid A)

Fig. 1a shows the typical SEM image of ZnO NRs on ITO substrate, which shows that ZnO NRs are well aligned and uniform

over a large scale. The density of ZnO NRs is estimated to be about 200/μm^2. The diameter of ZnO NRs is in the range of 25–50 nm, and the length is in the range of 200–300 nm. We have tried different substrates for growing ZnO nanorods, for example, glass, n-type Si (1 0 0) and sapphire substrates. It is found that growth of ZnO nanorods is substrate-independent as long as the substrate has a flat surface. Fig. 1b–f shows the morphology of the ZnO–Au hybrids (hybrid A) prepared under different Au deposition time. When the Au deposition time is 2 min, Au nanoparticles (NPs) are coated on the surfaces of ZnO NRs. The average diameter of Au NPs was about 5 nm. The interparticle distance between Au NPs is about 5 nm. The density of Au NPs on the surface of ZnO NRs was estimated to be about $2 \times 10^5/\mu m^2$. The as-prepared ZnO–Au hybrid is very similar to that prepared by a hydrothermal method [20]. In this reference, the size and density of Au NPs are dependent on the $HAuCl_4$ concentration. When the concentration of $HAuCl_4$ was 0.45 mM, Au NPs (10 nm of diameter) were attached uniformly on the surface of ZnO NRs. When the concentration of $HAuCl_4$ was decreased, lower density of Au NPs were located on the surface of ZnO NRs [20]. While in this work, the modification of Au NPs is influenced by Au deposition time, and the Au NPs prefer to link together to exist as a film when the Au deposition time is more than 6 min, which can be seen in Fig. 1d–f. The thickness of Au film can be calculated by comparing the diameters of ZnO–Au hybrid and pure ZnO NRs. The thicknesses of Au film with different Au deposition time are summarized in Table 1. It reveals that the thickness of Au film increases with increasing Au deposition time, and the film becomes more smoother when Au deposition time is more than 6 min. It should be noted that the hybrids with Au deposition time of 2 min, 4 min, 6 min, 8 min, and 10 min are marked as A2, A4, A6, A8, and A10, respectively.

The energy-dispersive X-ray spectroscopy (EDS) spectrum reveals that the ZnO NRs is composed of the elements of Zn and O (Fig. 2a). The signal of Zn and O are attributed to the ZnO NRs, and the In signal is from the ITO substrate. No other signals are observed in the EDS, indicating that the as-prepared sample is pure ZnO NRs. The EDS spectrum in Fig. 2a reveals that the as-prepared ZnO–Au hybrid (A2) is composed of the elements of Zn, O and Au. The signals of both Zn and O are attributed to the ZnO NRs. The Au signal results from the Au film on the surface of the ZnO NRs, and the In signal is from the ITO substrate. No other signals are observed in the EDS, indicating that the as-prepared sample is pure. Fig. 2b shows the X-ray diffraction (XRD) patterns of the ZnO NRs arrays and ZnO–Au hybrid (A2), in which the diffraction peaks from ITO were marked by a symbol ▼. For the ZnO NRs arrays, all the diffraction peaks can be indexed to the hexagonal wurtzite structure of bulk ZnO (JCPDS No. 36-1451). The peaks located at $2\theta = 34.7^\circ, 45.7^\circ, 63.2^\circ$ correspond to (0 0 2), (1 0 2) and (1 0 3) ZnO wurtzite structure facets, respectively. The predominant ZnO peak from the (0 0 2) plane indicates that the ZnO NRs arrays were grown with *c*-axis orientation normal to the substrate surface. For ZnO–Au hybrid (A2), another signals were observed at $2\theta = 38.4^\circ$ and 44.5°, which can be ascribed to the (1 1 1) and (2 0 0) planes of face-centered cubic Au crystals, respectively. The above results clearly indicate that Au NPs have been coated on the surface of ZnO NRs without impurities.

3.2. Fabrication and characterization of ZnO–Au nanocomposites (hybrid B)

Hybrid B was fabricated by a simple one-step chemical method. Briefly, the ITO slides with hybrid A (A2, A4, A6, A8, and A10) were immersed in a diluted HCl acid solution (1 mM) for 3 min. Then the hybrid B (B2, B4, B6, B8, and B10) was obtained after washing with water and drying under N_2. As a control experiment, pure ZnO NRs on the ITO slide was immersed in the 1 mM HCl acid solution for 3 min. The white color on ITO becomes transparent, which reveals

Table 1
The diameter of hybrid A and thicknesses of Au film with different Au deposition times.

Au deposition time (min)	2	4	6	8	10
Diameter of hybrid A (nm)	40	60	80	90	100
Thickness of Au film (nm)	10	30	50	60	70

that ZnO NRs have been etched completely by HCl. The XRD and SEM results indicate that none of ZnO NRs exist on the ITO slide (data not shown). Fig. 4 shows the SEM images of the as-prepared hybrid B. As observed from Fig. 4a, sparsely dispersed NRs were obtained after removing ZnO NRs from the ZnO–Au hybrid (A2) by HCl aqueous solution. There are some nanoparticles with diameter of 15 nm dispersed on the ITO surface. It can be seen that the density of NRs decreases (for B2 and B4), but the size is unchanged (for B2-10) after treating with HCl solution (shown in Fig. 1b). The density decreasing of NRs reveals that there is no continuous Au film formed on the ZnO NRs to resist acid etching for shorter Au deposition time (2 and 4 min). The density of NRs is estimated to be about 35/μm^2. The average diameter of B2 is about 40 nm, which is the same with that of A2. Fig. 4b shows NRs with helical structure at the bottom, and the density of NRs was estimated to be about 50/μm^2. The average diameter of NRs was 60 nm. Fig. 4c–e shows SEM images of hybrids (B6, B8, B10) with Au film thickness of 50, 60 and 70 nm, respectively, which is corresponding to the Au deposition time of 6, 8, and 10 min, respectively. The density and size of NRs in hybrid B are summarized in Table 2. From Table 2, it reveals that the density

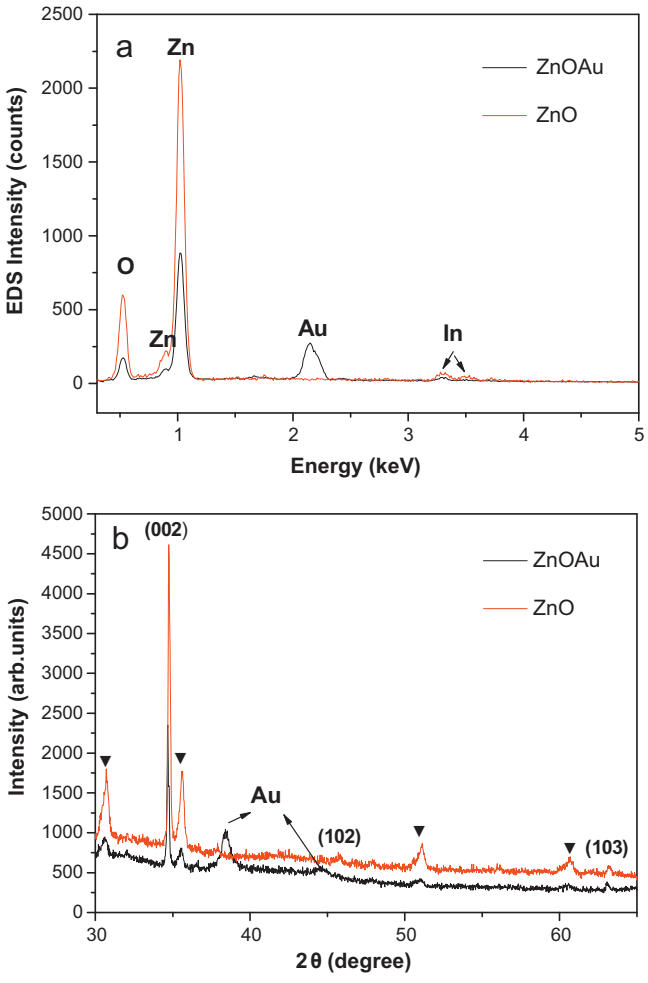

Fig. 2. (a) EDS spectra and (b) XRD patterns of ZnO NRs and ZnO–Au hybrid A2.

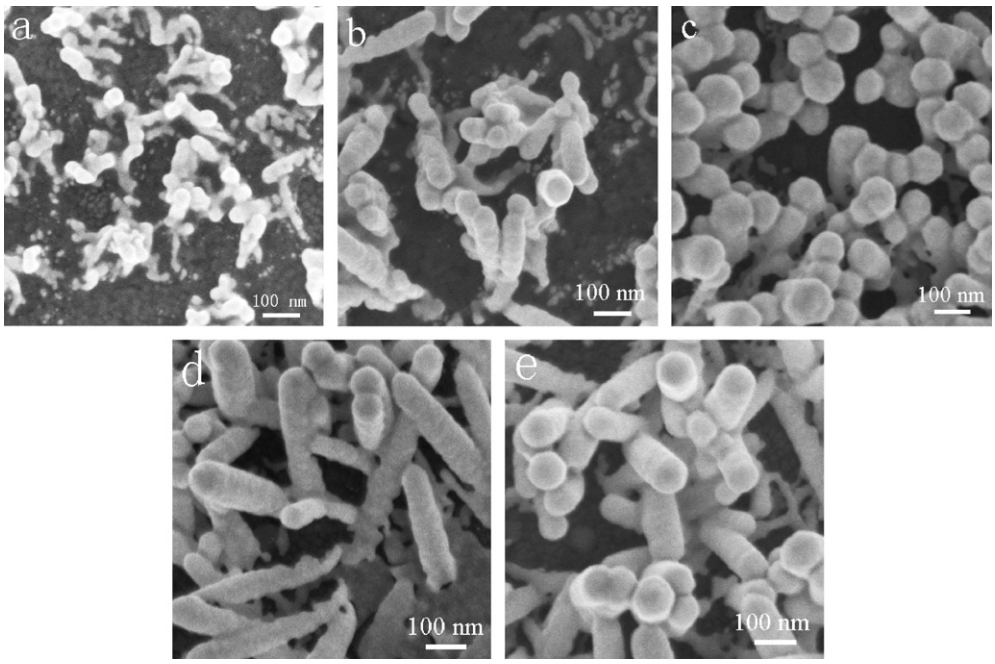

Fig. 3. SEM images of (a) ZnO–Au hybrid B with different Au deposition times (b) 2 min, (c) 4 min, (d) 6 min, (e) 8 min, (f) 10 min.

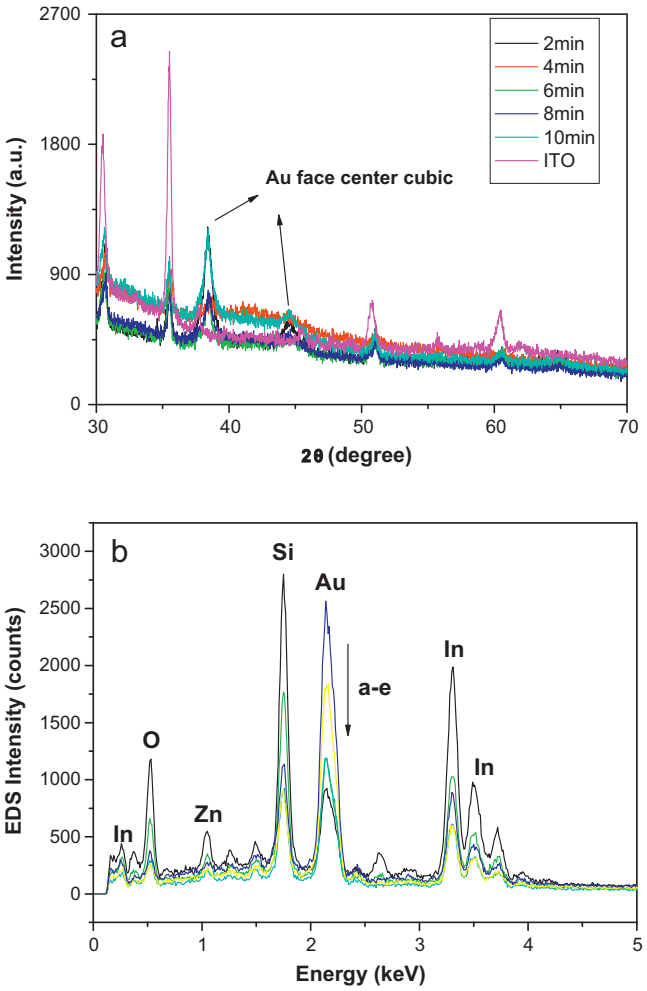

Fig. 4. (a) XRD patterns and (b) EDS spectra of ZnO–Au hybrid B.

and size of hybrids are increased with increasing the Au deposition time.

The purity and crystalline of the as-synthesized hybrids B were examined by X-ray diffraction (XRD) patterns. Fig. 4a shows the XRD patterns of the hybrid B with different Au deposition times and ITO slide. The 2θ diffraction peaks at 38.3° and 44.5° corresponded to (1 1 1) and (2 0 0) plane of the face center cubic of Au. The peak intensity of Au increases with the increasing of Au deposition time. But the diffraction peaks related to ZnO are not observed. From SEM and XRD analyses, the hybrid B mainly consists of Au mesocrystals. To further confirm the structure of hybrid B, EDS was used to determine the element of hybrid B (Fig. 4b). It reveals that the hybrids consist of element Zn, O and Au, and the In signal is from the ITO substrate. The signals of Zn are both attributed to the $ZnCl_2$ and surviving ZnO tightly covered by Au film. It reveals that some ZnO NRs exist in the center of Au films, as the EDS peak intensity of Zn decreases with the increasing of Au deposition time. From above results, it is reasonable to conclude that the hybrid B is comprised Au mesocrystals as the shell with a few ZnO NRs as the core.

3.3. The optical properties of hybrid B

Fig. 5 shows the room temperature PL (RTPL) spectra of ZnO NRs and ZnO–Au nanocomposites (hybrid B). The RTPL spectrum of pure ZnO NRs shows a UV emission at ~378 nm associated with its exciton emission and a broad band related to defects ranged from 500 to 700 nm in the visible light. The broad band may be caused by discrepancies, such as O vacancies, Zn vacancies, Zn interstitials, O interstitials, donor acceptor pairs, and surface state [22,23]. After being decorated with 10 nm Au NPs followed by corrosion with diluted HCl solution, the Au mesocrystals display weakened and red-shifted UV (390 nm) and blue-shifted visible

Table 2
The diameter and density of Au mesocrystals with different Au deposition times.

Au deposition time (min)	2	4	6	8	10
Diameter of Au mesocrystals (nm)	40	60	80	90	100
Density of Au mesocrystals (per μm^2)	35	50	80	85	90

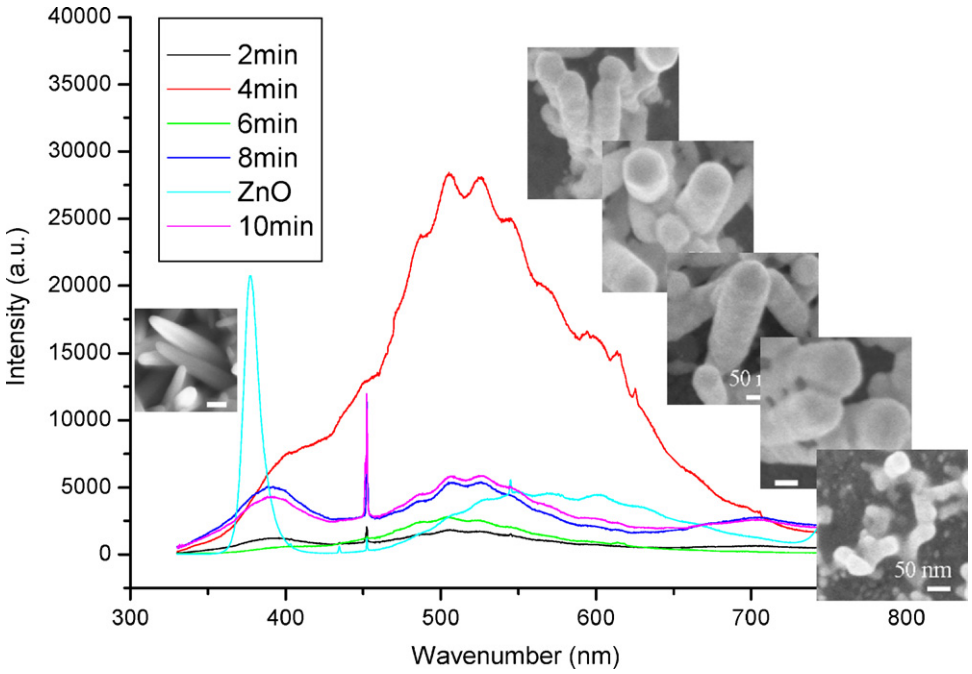

Fig. 5. The RTPL spectra of ZnO NRs and ZnO–Au hybrid B with different Au deposition times the inset shows the corresponding SEM images.

(450–600 nm) emission. The Au mesocrystals (B2, B6) with 10 and 50 nm of thickness exhibit two weaker emissions at both UV (396 nm) and visible range from 400 to 600 nm. For Au mesocrystals (B8, B10) with 60 and 70 nm of thickness, they both exhibit weakened UV emission (390 nm) and slightly enhanced visible emission (450–600 nm). Interestingly, the Au mesocrystals (B4) with 30 nm of thickness display a highly enhanced visible emission and a significantly quenched UV emission. It should be noted that the thickness of Au mesocrystals is proportional to Au deposition time, which is shown in Table 1. It can be found from Fig. 5 that the UV emission of Au mesocrystals is weakened than pure ZnO NRs, and the Au mesocrystals with 30 nm (B4) of thickness display the weakest UV emission. ZnO visible emission is sensitive to thickness of Au mesocrystals, which is controlled by Au deposition time. An obvious trend is that the ratios of the visible and UV emission band heights increased strongly with the increasing thickness film, achieves maximum value (~4.8) for hybrid B4. The results indicate that Au mesocrystals with 30 nm of thickness revealed greater white emission than other mesocrystals.

In previous work on constructing ZnO–Au hybrid, Au NPs were adsorbed or grown on ZnO surface by chemical method [17,19,24]. For example, Chen et al. firstly synthesized Au NPs of different sizes by the well-established citrate reduction method. And then they fabricated ZnO–Au hybrid structures by incubating ZnO NWs in concentrated Au NPs solution at room temperature for 12–18 h [17]. Chang et al. prepared ZnO–Au hybrid by immersing ZnO NWs into $HAuCl_4$ solution under UV light for 4 min [24]. Wang et al. immersed ZnO NRs into an aqueous solution of $HAuCl_4$ in the presence of 1.25 mM $CoCl_2$ for 1 min to deposit Au NPs onto the outerwall of NRs [19]. In their work, ZnO NRs act as the major part and Au NPs act as a very thin layer to modify the ZnO surface. The electron transfer from the defect sites on the ZnO surfaces to Au, which can suppress other radiations. This charge transfer is related to the formation of a Schottky barrier and a depletion layer between the ZnO NWs and the Au NP, since the work function of ZnO (4.3 eV) is smaller than that of Au (5.1 eV). Thus the UV emission of ZnO NRs (or NWs) is enhancement after adsorbing Au NPs. On the other hand, Au NPs have a strong absorption in the visible range, which may contribute to the quenching of visible emission of ZnO NRs. Therefore, the visible emission is much weakened after attaching Au NPs onto ZnO NRs. Our system is significantly different with previous work, because in the present study most of ZnO NRs were etched by HCl, and the outerwall of surviving ZnO were covered with relatively thick Au films. Both etching of ZnO by acid and covering of Au film induce many defects on the surface of ZnO NRs. The surface modification makes energy potential low enough to promote surface states trapping the photo-generated electrons or holes, which paves the pathway to form luminescence centers.

Control experiments without HCl etching were carried out to isolate and to evaluate the effects of etching process. As illustrated in Fig. 6, UV and visible emission were both weakened after covering with Au NPs. And there is an obvious red shift of the UV peak after the Au deposition, which might be a result of a higher density of surface defects [25]. As shown in Fig. 6, the red-shifts become more obvious when increasing the Au deposition time from 2 to 10 min, which can be explained by the increase of surface defects. As known that Au NPs had a strong absorption in the visible range, which may contribute to the quenching of visible emission of ZnO

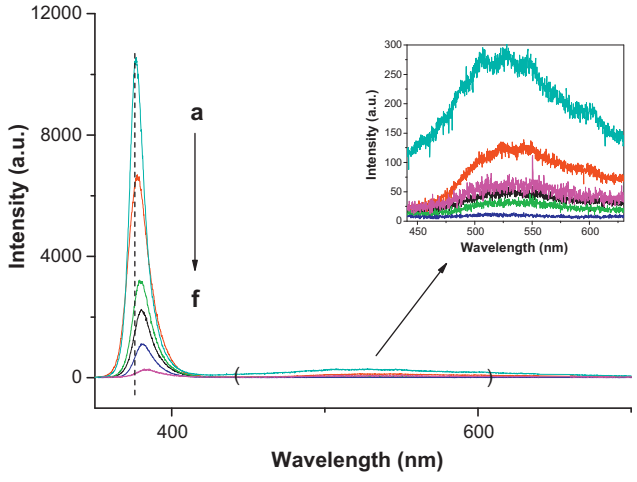

Fig. 6. The RTPL spectra of ZnO NRs and ZnO–Au hybrid A without HCl etching.

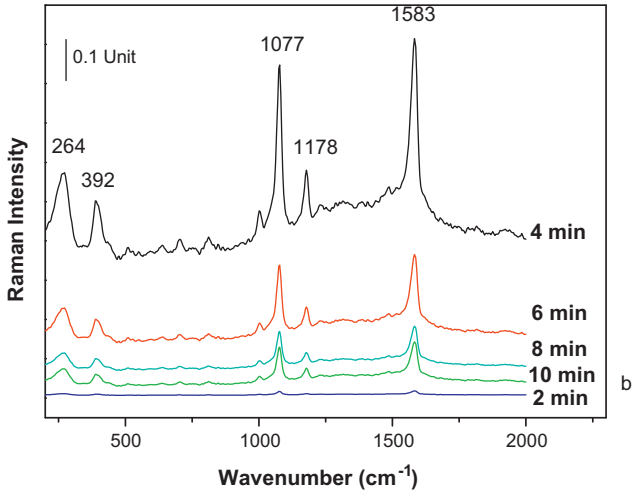

Fig. 7. Typical FT-SERS spectra of 4-ATP (1×10^{-5} M) on ZnO–Au hybrid A with different Au deposition times.

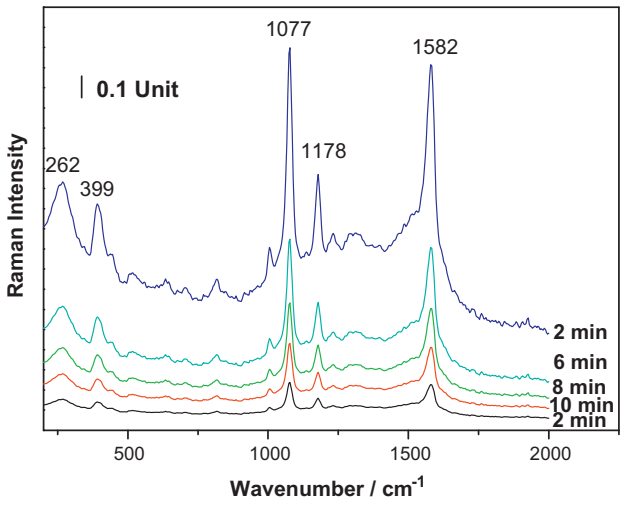

Fig. 8. Typical FT-SERS spectra of 4-ATP (1×10^{-5} M) on ZnO–Au hybrid B with different Au deposition times.

NRs when Au NPs were introduced. This result excluded Au NPs as the origin of the visible emission and confirms the etching role in inducing more defects on surviving ZnO surface. In general, without etching, the intensity of UV and visible emission are both largely quenched, which further reflects the effectiveness of Au mesocrystals with little ZnO in the internal-wall. In addition, it should be noted that the PL properties of ZnO NRs and ZnO–Au hybrids (A and B) are reproducible, which have been confirmed by measuring different samples, and several points for each sample.

From above results, it demonstrated that the modification of Au on ZnO NRs could not enhance but quench the visible emission of ZnO NRs. We suggest that the enhanced visible emission is caused by the presence of $ZnCl_2$ at the interface between ZnO cores and Au shells. $ZnCl_2$ composites are formed after acid treating of ZnO/Au hybrid A, which has been confirmed from XRD and EDS analysis. The presence of $ZnCl_2$ on ZnO cores increases the defects of oxygen and zinc vacancies. Recent works have relevant discussions on ZnO defects on undoped ZnO and doped ZnO by Eu [26,27]. To completely understand that how the visible emission is dramatically enhanced after the Au decoration and acid treating, further work on both experiments and calculations are needed in the future.

3.4. SERS measurements of 4-ATP molecules on the hybrids A and B

In our previous studies, we investigated the assembly of Ag NPs on the ZnO NRs arrays, and explored the applications of these ZnO–Ag nanocomposites in the SERS-active substrate primarily [28]. For one basic application, we also hope these ZnO–Au hybrids formed in this work can be used as SERS-active substrates. In order to detect the possibility of these hybrids A for the applications in SERS-active substrates, 20 μL 1×10^{-5} M 4-ATP (dissolved by ethanol) was dropped onto these substrates and detected with FT-Raman spectrometer. Fig. 7 gives typical comparative FT-SERS spectra of 1×10^{-5} M 4-ATP on hybrids shown in Fig. 1b–f. It is obvious that the ZnO–Au hybrid with 30 nm thickness of Au film shows greater enhancement ability than the other hybrids for 4-ATP probe molecules. And no Raman peaks could be observed when the 4-ATP solution was dispersed on pure ZnO NRs substrate. An obvious trend is that the enhancement ability firstly increases and then decreases with the increase of Au film thickness. As mentioned above, the Au film thickness is dependent on the Au deposition time, thus the SERS intensity of ZnO–Au hybrids can be controlled by tuning Au deposition time. In these SERS spectra, four important bands, υ(CC) for 1583 cm^{-1}, υ(CC) for 1077 cm^{-1}, δ(CH) for 1178 cm^{-1}, and 392 cm^{-1} which is assigned to one of the vibrational modes of C—S bond, are all dominated with the in-plane (a_1) vibrational mode [29–31]. Similar results have been reported by Wang et al. who considered the predominance of a_1 mode in the FT-SERS spectra might imply the enhancement via the electromagnetic mechanism is significant [32]. Fig. 8 shows the typical FT-SERS spectra of 1×10^{-5} M 4-ATP on hybrids B shown in Fig. 3, in which similar trend in the enhancement ability with that of hybrid A is observed.

We suggest that the size and interparticle distance are two main factors for the enhancement ability of SERS. It can be seen from Fig. 1 that the diameter of Au NPs is about 5 nm when Au deposition time is 2 min. It is reported that the most enhanced SERS often presents on aggregated silver nanoparticles in the range of 20–200 nm [33], thus the hybrid prepared under 2 min deposition time shows the weakest SERS signal. The hybrid prepared under 4 min deposition time displays the strongest SERS signals, in which Au NPs are closely spaced and interparticle distance is smaller than 2 nm. Similar results have been reported by Xu et al., who have calculated and suggested that closely spaced nanoparticles separated by 1 nm can provide an enhancement of 10^{10} at the interstitial of two NPs [34]. While the SERS intensity decreases when further increasing Au deposition time, which can be explained by the "hot spot" mechanism. In previous work, large enhancement was observed for aggregates with multiple particles, but little enhancement was found for single nanoparticles [35]. This is because there are many "hot spots" at junction sites between aggregated NPs, in which huge electromagnetic field enhancements are caused by plasmon coupling between nanoparticles in close proximity [36]. In our work, Au NPs linked together and became continuous films in hybrids when increasing deposition time (from 6 to 10 min), which decreased the "hot spots" and decreased the SERS intensity.

The electric beam evaporation deposition method provided in this work maybe a feasible strategy for the preparation of SERS-active substrates for the practical applications in chemical and biological analysis. Firstly, the good signal-to-noise for the SERS spectra of 4-ATP on the hybrids indicate that these substrates are very suitable as SERS substrates. In this work, we thought the Raman enhancement mainly come from three factors: the rough surface on nanometer scale, SERS "hot spots" between two close-packed Au NPs, and the relatively large surface area provided by ZnO NRs templates. Secondly, the ZnO–Au hybrids prepared by combining hydrothermal method and electric beam evaporation deposition method have good stability and reproducibility. Finally,

this one-step electric beam evaporation deposition method to prepare Au NPs aggregates and film for SERS applications is very simple and quick.

4. Conclusions

We have developed a simple method to controllable fabricate white emission ZnO–Au hybrid nanostructures by combining hydrothermal method and electric beam evaporation deposition technology and post-treating with acid. The white emission intensity is dependent on the Au deposition time, and the highest white emission is obtained for Au mesocrystals (deposition time is 4 min). It is suggested that the thickness of Au mesocrystals is proportional to Au deposition time, and the thickness of Au mesocrystals is a main factor for white emission. Control experiments revealed that the etching with HCl plays an important role in enhancing the white emission. In addition, the ZnO–Au hybrids can be used as SERS substrates for detection of 4-ATP molecules, which provides an opportunity to fabricate stable and reproducible SERS-active substrates.

Acknowledgment

This work was supported by the Natural Science Foundation for the Youth of China under Grant No. 21101146.

References

[1] T. Mokari, E. Rothenberg, I. Popov, R. Costi, U. Banin, Selective growth of metal tips onto semiconductor quantum rods and tetrapods, Science 304 (2004) 1787–1790.
[2] A.G. Dong, J. Chen, P.M. Vora, J.M. Kikkawa, C.B. Murray, Binary nanocrystal superlattice membranes self-assembled at the liquid–air interface, Nature 466 (2010) 474–477.
[3] A.M. Smith, S.M. Nie, Semiconductor nanocrystals: structure, properties, and band gap engineering, Accounts of Chemical Research 43 (2010) 190–200.
[4] M. Kazes, D.Y. Lewis, U. Banin, Method for preparation of semiconductor quantum-rod lasers in a cylindrical microcavity, Advanced Functional Materials 14 (2004) 957–962.
[5] C. Xu, J. Xie, D. Ho, C. Wang, N. Kohler, E.G. Walsh, J.R. Morgan, Y.E. Chin, S.H. Sun, Au–Fe_3O_4 dumbbell nanoparticles as dual functional probes, Angewandte Chemie International Edition 47 (2008) 173–176.
[6] J.S. Choi, Y.W. Jun, S.I. Yeon, H.C. Kim, J.S. Shin, J. Cheon, Biocompatible heterostructured nanoparticles for multimodal biological detection, Journal of the American Chemical Society 128 (2006) 15982–15983.
[7] V. Salgueirino-Maceira, M.A. Correa-Duarte, Increasing the complexity of magnetic core/shell structured nanocomposites for biological applications, Advanced Materials 19 (2007) 4131–4144.
[8] H. Yu, S. Chen, P.M. Rice, S.X. Wang, R.L. White, S. Sun, Dumbbell-like bifunctional Au–Fe_3O_4 nanoparticles, Nano Letters 5 (2005) 379–382.
[9] B.O. Dabbousi, J. Rodriguez-Viejo, F.V. Mikulec, J.R. Heine, H. Mattoussi, R. Ober, K.F. Jensen, M.G. Bawendi, (CdSe)ZnS core–shell quantum dots: synthesis and characterization of a size series of highly luminescent nanocrystallites, Journal of Physical Chemistry B 101 (1997) 9463–9475.
[10] P. Li, Z. Wei, T. Wu, Q. Peng, Y.D. Li, Au–ZnO hybrid nanopyramids and their photocatalytic properties, Journal of the American Chemical Society 133 (2011) 5660–5663.
[11] J.S. Lee, E.V. Shevchenko, D.V. Talapin, Au-PbS core–shell nanocrystals: plasmonic absorption enhancement and electrical doping via intra-particle charge transfer, Journal of the American Chemical Society 130 (2008) 9673–9675.
[12] X.M. Zhao, B.H.K.L.A. Zhang, G. Zhang, L.Y. Cao, X.J. Liu, H.M. Sun, H.S. Wang, L.H. Lu, Monitoring catalytic degradation of dye molecules on silver-coated ZnO nanowire arrays by surface-enhanced Raman spectroscopy, Journal of Materials Chemistry 19 (2009) 5547–5553.
[13] H.B. Zeng, P.S. Liu, W.P. Cai, S.K. Yang, X.X. Xu, Journal of Physical Chemistry C 112 (2008) 19620.
[14] X.H. Li, G.Y. Chen, L.B. Yang, Z. Jin, J.H. Liu, Multifunctional Au-coated TiO_2 nanotube arrays as recyclable SERS substrates for multifold organic pollutants detection, Advanced Functional Materials 20 (2010) 2815–2824.
[15] U. Ozgur, Y.I. Alivov, C. Liu, A. Teke, M.A. Reshchikov, S. Dogan, V. Avrutin, S.J. Cho, H. Morkoc, A comprehensive review of ZnO materials and devices, Journal of Applied Physics 98 (2005) 041301.
[16] G.Y. Shan, S. Wang, X.F. Fei, Y.C. Liu, G.L. Yang, Heterostructured ZnO/Au nanoparticles-based resonant Raman scattering for protein detection, Journal of Physical Chemistry B 113 (2009) 1468–1472.
[17] T. Chen, G.Z. Xing, Z. Zhang, H.Y. Chen, T. Wu, Tailoring the photoluminescence of ZnO nanowires using Au nanoparticles, Nanotechnology 19 (2008) 435711.
[18] V. Dhas, S. Muduli, W. Lee, S.H. Han, S. Ogale, Enhanced conversion efficiency in dye-sensitized solar cells based on ZnO bifunctional nanoflowers loaded with gold nanoparticles, Applied Physics Letters 93 (2008) 243108.
[19] Q. Wang, B.Y. Geng, S.Z. Wang, ZnO/Au hybrid nanoarchitectures: wet-chemical synthesis and structurally enhanced photocatalytic performance, Environmental Science and Technology 43 (2009) 8968–8973.
[20] L.L. Sun, D.X. Zhao, Z.M. Song, C.X. Shan, Z.Z. Zhang, B.H. Li, D.Z. Shen, Gold nanoparticles modified ZnO nanorods with improved photocatalytic activity, Journal of Colloid and Interface Science 363 (2011) 175–181.
[21] Y.J. Lee, D.S. Ruby, D.W. Peters, B.B. Mckenzie, J.W.P. Hsu, ZnO nanostructures as efficient antireflection layers in solar cell, Nano Letters 8 (2008) 1501–1505.
[22] P.H. Kasai, The yellow luminescence of zinc oxide, Solid State Commnunications 102 (1997) 359–363.
[23] H.J. Egelhaaf, D. Oelkrug, Luminescence and nonradiative deactivation of excited states involving oxygen defect centers in polycrystalline ZnO, Journal of Crystal Growth 161 (1996) 190–194.
[24] S.J. Chang, T.J. Hsueh, I.C. Chen, B.R. Huang, Highly sensitive ZnO nanowire CO sensors with the adsorption of Au nanoparticles, Nanotechnology 19 (2008) 175502.
[25] A.B. Djurisic, Y.H. Leung, Optical properties of ZnO nanostructures, Small 2 (2006) 944–961.
[26] D.D. Wang, G.Z. Xing, M. Gao, L.L. Yang, J.H. Yang, T. Wu, Eefects-mediated energy transfer in red-light-emitting Eu-doped ZnO nanowire arrays, Journal of Physical Chemistry C 115 (2011) 22729–22735.
[27] G.Z. Xing, D.D. Wang, J.B. Yi, L.L. Yang, M. Gao, M. He, J.H. Yang, J. Ding, T. Chien Sum, T. Wu, Correlated d^0 ferromagnetism and photoluminescence in undoped ZnO nanowires, Applied Physics Letters 96 (2010) 112511.
[28] L.L. Sun, D.X. Zhao, Z.Z. Zhang, B.H. Li, D.Z. Shen, DNA-based fabrication of density-controlled vertically aligned ZnO nanorod arrays and their SERS applications, Journal of Materials Chemistry 21 (2011) 9674–9681.
[29] M. Osawa, N. Matsuda, K. Yoshii, I. Uchida, Charge transfer resonance Raman process in surface-enhanced Raman scattering from p-aminothiophenol adsorbed on silver: Herzberg–Teller contribution, Journal of Physical Chemistry B 98 (1994) 12702–12707.
[30] J. Zheng, X. Li, R. Gu, T. Lu, Comparison of the surface properties of the assembled silver nanoparticle electrode and roughened silver electrode, Journal of Physical Chemistry B 106 (2002) 1019–1023.
[31] X. Hu, W. Cheng, T. Wang, Y. Wang, E. Wang, S. Dong, Fabrication, haracterization, and application in SERS of self-assembled polyelectrolyte–gold nanorod multilayered films, Journal of Physical Chemistry B 109 (2005) 19385–19389.
[32] T. Wang, R. Zheng, X. Hu, L. Zhang, S. Dong, Templated assembly of gold nanoparticles into microscale tubules and their application in surface-enhanced Raman scattering, Journal of Physical Chemistry B 110 (2006) 14179–14185.
[33] D.J. Maxwell, S.R. Emory, S. Nie, Nanostructured thin-film materials with surface-enhanced optical properties, Chemistry of Materials 13 (2001) 1082–1088.
[34] H.X. Xu, E.J. Bjerneld, M. Kall, L. Borjesson, Spectroscopy of single hemoglobin molecules by surface enhanced Raman scattering, Physical Review Letters 83 (1999) 4357–4360.
[35] A.M. Michaels, J. Jiang, L. Brus, Ag nanocrystal junctions as the site for surface-enhanced Raman scattering of single rhodamine 6G molecules, Journal of Physical Chemistry B 104 (2000) 11965–11971.
[36] L.L. Sun, D.X. Zhao, M. Ding, Z.K. Xu, Z.Z. Zhang, B.H. Li, D.Z. Shen, Controllable synthesis of silver nanoparticle aggregates for surface-enhanced Raman scattering studies, Journal of Physical Chemistry C 115 (2011) 16295–16304.